Quaternary Research (2025), **125**, 87–103
doi:10.1017/qua.2024.62

Research Article

Near-surface winds at the southern Laurentide ice margin through the last deglaciation

Jessica L. Conroy[a], Christina Karamperidou[b], and David A. Grimley[c]

[a]Department of Earth Science & Environmental Change, University of Illinois Urbana-Champaign, Urbana, IL; [b]Department of Atmospheric Sciences, University of Hawaii at Manoa, Honolulu, HI and [c]Illinois State Geological Survey, Prairie Research Institute, University of Illinois Urbana-Champaign, Champaign, IL

Abstract

Terrestrial proxies of wind direction spanning the last deglaciation suggest easterly winds were present near the Laurentide Ice Sheet margin in the North American midcontinent. However, the existence and spatial extent of such easterly winds have not been investigated with transient paleoclimate model simulations, which could provide improved dynamical context for interpreting the causes of these winds. Here we assess near-surface winds near the retreating southern Laurentide Ice Sheet margin using iTRACE, a transient simulation of deglacial climate from 20–11 ka. Near the south-central margin, simulated near-surface winds are northeasterly to easterly through the deglaciation, due to katabatic flow off the ice sheet and anticyclonic circulation. As the ice sheet retreats and the Laurentide High moves northeastward and weakens, near-surface northeasterly winds weaken. Meltwater fluxes also influence temperature and sea level pressure over the North Atlantic, leading to easterly wind anomalies over eastern to midwestern North America. The agreement between proxy and model wind directions is promising, although simulated easterly to northeasterly winds extend too far south in iTRACE relative to the proxy data. Agreement is also strongest in winter, spring, and fall, suggesting these may have been seasons with greater aeolian activity.

Keywords: Proxy–model comparison; last deglaciation; paleowind; loess; dunes; climate model

Introduction

Wind is a fundamental component of the climate system, driven by the large-scale atmospheric circulation, and is intricately linked to near-surface climate variables as well as remote atmospheric teleconnections (St. George and Wolfe, 2009; McVicar et al., 2012). As wind power becomes a progressively larger component of energy production, understanding variability in wind, its drivers, and how wind properties are expected to vary in the future with increased greenhouse gas forcing is increasingly relevant. However, future assessments of wind speed and wind power are uncertain. With future anthropogenic forcing, there is evidence for spatially variable changes in wind speed, and subsequently wind power, in many areas (Karnauskas et al., 2018; Martinez and Igelsias, 2022). There is also a wide range of twenty-first century wind speed trends across model simulations, as well as a wide range of agreement between simulated twentieth to twenty-first century wind speed and observed (re-analysis) wind speed (Karnauskas et al., 2018; Martinez and Iglesias, 2022). Furthermore, the nature of recent trends in observed wind speed and their relationship to natural and anthropogenic forcing factors is still unclear. For example, there is emerging evidence that the recent wind 'stilling' phenomena may be reversing, demonstrating that regional wind speeds vary on multidecadal timescales with ocean–atmosphere forcing (Zeng et al., 2019).

Although wind speed is the most assessed wind property, wind direction changes can also provide information on changes in large-scale atmospheric circulation. Past near-surface wind directions have been inferred from aspects of various types of geologic materials on the earth surface, including orientation of dunes and spits, as well as mapped patterns of loess thickness, grain size, and chemistry (e.g., Muhs and Bettis, 2000; Sweeney et al., 2004; Mason et al., 2011; Markewich et al., 2015; Schaetzl et al., 2018; Vimpere, 2023). These wind-direction archives, which cover extensive areas in mid-latitude regions, can enable inquiries into the past nature of atmospheric circulation during times of radically different climate forcing, such as the last glacial maximum (LGM). In addition, they also provide an avenue to test model simulations of past wind direction, often revealing encouraging consistency in modeled and proxy-inferred paleowind direction (Sweeney et al., 2004; Mason et al., 2011).

With the development of the Paleoclimate Modeling Intercomparison Projects (PMIP), comparison of proxy wind direction records with multiple model simulations of paleoclimates is now possible. For example, LGM wind directions were assessed in both wind-direction proxies and models participating in the LGM experiment of PMIP3 for midcontinental and southeastern North America (Conroy et al., 2019). This study found a range of proxy data–model agreement with respect to the direction of LGM winds, and concluded that the Laurentide High, the region of stationary high pressure over the Laurentide

Corresponding author: Jessica L. Conroy; Email: jconro@illinois.edu

Cite this article: Conroy, J.L., Karamperidou, C., Grimley, D.A., 2025. Near-surface winds at the southern Laurentide ice margin through the last deglaciation. *Quaternary Research* **125**, 87–103. https://doi.org/10.1017/qua.2024.62

Ice Sheet, was weaker, with a smaller spatial footprint, in climate models that agree best with proxy wind-direction data (Conroy et al., 2019). Another recent study compared proxy wind directions from a range of past time periods versus modern wind direction and concluded that near-surface wind directions have remained largely unchanged in the Late Quaternary (Vimpere, 2023).

The majority of wind-direction proxy records from midcontinental and southeastern North America revealed overall westerly to northwesterly near-surface winds during the maximum extent of Wisconsin Episode glaciation (Muhs and Bettis, 2000; Conroy et al., 2019). A general consensus for this time period, and of the LGM globally, based on ice sheet extent, sea level, and solar insolation, is approximately 27–19 cal ka (Clark et al., 2009), and these wind-direction archives generally span this time range. However, following the LGM, some paleowind-direction records in North America suggest an easterly component to near-surface winds (Wolfe et al., 2004; Arbogast et al., 2015; Schaetzl et al., 2018). Because these data mainly span the deglacial timeframe (generally after 19 cal ka), they were not included in previous LGM proxy data–model wind direction analyses. These records are largely from the Upper Midwest and western Canada, near the retreating Laurentide Ice Sheet margin, and support easterly winds within ∼150 km of the ice sheet margin during the deglaciation (Wolfe et al., 2004; Arbogast et al., 2015; Schaetzl et al., 2018).

Here we further examine proxy data–model paleowind direction agreement in North America, using a transient model simulation from 20 ka to 11 ka to assess wind changes during a time of rapid but punctuated glacial retreat and overall warming (He et al., 2021), including significant meltwater events. First, we describe the simulated spatial and temporal changes in near-surface wind direction from 20 ka to 11 ka in the iTRACE modeling experiments. Next, using iTRACE model experiments with and without the inclusion of meltwater forcing, we describe the effect of deglacial meltwater pulses on near-surface winds. Finally, we assess how well wind direction in this transient model simulation agrees with deglacial proxy wind direction over 1-ka intervals.

Methods

iTRACE model data

The iTRACE simulation was performed with the isotope-enabled Community Earth System Model (iCESM) version 1.3, which couples the Community Atmosphere Model version 5.3 (CAM5.3), the Community Land Model version 4 (CLM4), the Parallel Ocean Program version 2 (POP2) ocean model, and the Los Alamos Sea Ice Model version 4 (CICE4) (Hurrell et al., 2013; Brady et al., 2019; He et al., 2021). The model has 1.9° latitude by 2.5° longitude spatial resolution with 30 vertical levels in the atmosphere. In this work we only assessed physical climate variables, excluding the model isotope data, but both modern climate and isotope simulations with CESM have been well vetted against modern climate and isotope observations (Hurrell et al., 2013; Brady et al., 2019). Four 'sensitivity runs' of the transient climate from 20 ka to 11 ka were performed in 1000-year increments to isolate the climate response to key forcing factors, similar to the previous transient deglacial climate simulations of Trace-21ka (Liu et al., 2009). These include 'ICE', which imposes the ICE-6G-C dataset, with the modeled ice sheet and land fraction changed every 1 ka (Peltier et al., 2015). 'ICE+ORB' adds orbital forcing (ORB) of radiation, 'ICE+ORB+GHG', adds atmospheric greenhouse gas (GHG) (CO_2, CH_4, N_2O) concentrations, and finally, 'ICE+ORB+GHG+MW' imposes meltwater fluxes (MW) in the northern and southern hemispheres that are prescribed to be 'consistent with sea level changes' beginning at 19 ka (He et al., 2021).

In this work we assessed the zonal and meridional winds, sea level pressure (SLP), and surface temperature variables over North America. Because near-surface winds are of primary interest, we designated the lowest atmosphere level in the model, 992.6 hPa (∼159–177 m for temperatures −10°C to 20°C), as indicative of the near surface, although we also investigated zonal wind through the troposphere. Although use of wind at 10-m height (U10) would have been preferred, the zonal and meridional components of 10-m wind were not archived from iTRACE, which hindered our ability to use U10 for wind-direction analysis. An evaluation of the direction of the fastest winds at a higher temporal frequency also would have been preferred, given that phenomena such as sand and silt entrainment require threshold wind velocities that may not have the same direction as the climatological mean wind speeds (e.g., Sweeney et al., 2008; Mason et al., 2011; Sweeney and Mason 2013). However, we were limited by available monthly mean model output for this exercise.

For each variable, we calculated seasonal climatologies for each 1-ka period and plotted annually resolved time series of key variables in select regions. We also assessed the difference in variables from the ICE+ORB+GHG and ICE+ORB+GHG+MW experiments in order to isolate the effect of meltwater forcing on surface winds in the study region. The timing and location of meltwater pulses vary based on proxy evidence (see He et al., 2021; Fig. 2a). The largest and most prolonged meltwater pulses in the Northern Hemisphere occurred during Heinrich Stadial Event 1 (HS1, 18–14.5 ka), followed by the Younger Dryas (12.9–11.7 ka) episode, and are associated with substantial climate effects, which motivates our investigation. We focused our spatial assessment of meltwater effects on the 16-ka time slice, when Northern Hemisphere meltwater forcing is strongest (e.g., Oster et al., 2023), although we also examined meltwater effects in the 13-ka time slice, which includes meltwater associated with the Younger Dryas episode.

Proxy wind-direction data

Using the available, peer-reviewed literature, we assessed inferred wind direction from geomorphic features including dune and spit orientations, and patterns of loess thickness, grain size, and geochemistry across North America (Table 1). Spatially, we focused on collating data in the areas near the margin of the Laurentide and Cordilleran ice sheets, although the dataset includes proxy records from throughout the Mississippi–Missouri River Basin and the Atlantic Coastal Plain. Using the longitude and latitude of the published data, we placed records into 0.5° × 0.5° grids approximating their locations. Some published studies contain multiple sites that span multiple grids, whereas other grids may contain multiple, independent records. Proxy-inferred wind direction for each 0.5° × 0.5° grid was considered categorically, and separately, for both zonal and meridional winds. For example, if a record or records in a grid indicate westerly winds, a 'W' is indicated under the zonal wind column in Table 1. If there is no interpretation or indication of meridional wind direction, the associated cell is left blank in the meridional wind column in Table 1.

The issue of uncertainty in proxy wind direction is an important one. In particular, whereas the orientation of certain aeolian features such as dunes can be considered more quantitatively (i.e., in degrees), the interpretation of wind direction from loess is less certain. Loess thickness, grain size, and related geochemistry

https://doi.org/10.1017/qua.2024.62 Published online by Cambridge University Press

Table 1. North American proxy records of near-surface wind direction from the LGM and deglaciation. Sites and samples therein are organized in grids of 0.5° latitude × 0.5° longitude. Archive type abbreviations are as follows: LP = loess particle size trends, LT = loess thickness patterns, LC = loess chemistry, Dr = wind-aligned drainages, D = dune orientation, S = lacustrine spits, SaSt = sand stringers. Zonal wind direction indicates whether interpreted wind direction is westerly or easterly. Meridional wind direction indicates whether interpreted wind direction is northerly or southerly. A confidence level of 1 indicates more precise chronology and/or wind-direction information, whereas level 2 indicates more uncertainty in chronology and/or inferred wind direction. 'Secondary' references are previously published syntheses that included these wind-direction data.

	Latitude °N	Longitude °W	Archive Type	Age	Zonal Wind Direction (E or W)	Meridional Wind Direction (N or S)	Confidence Level	Primary Reference(s)	Secondary References
1	42	73	D, S	25–15 cal ka BP	E	N	2	Thorson and Schile (1995)	
2	42	73	D	14.6–12.9 cal ka BP	W	N	2	Thorson and Schile (1995)	
3	38.5	75.5	D	30–15 ka	W	N	2	Carver and Brook (1989)	Markewich et al. (2015); Conroy et al. (2019)
4	39.5	75.5	D	21.7 to 18.8 ka	W	N	1	Wolfe et al. (2023)	
5	34.5	78.5	D	30–15 ka	W	S	2	Carver and Brook (1989)	Markewich et al. (2015); Conroy et al. (2019)
6	33.5	79	D	30–15 ka	W	S	2	Carver and Brook (1989)	Markewich et al. (2015); Conroy et al. (2019)
7	45	80	S	13.2–11.5 ka	E	N	1	Shaetzl et al. (2016)	Schaetzl et al. (2018)
8	32.5	81	D	43.5–12.2 ka	W		1	Swezey et al. (2013)	Markewich et al. (2015)
9	32	82	D	30–15 ka	W		2	Ivester et al. (2001); Ivester and Leigh (2003)	Markewich et al. (2015); Conroy et al. (2019)
10	32.5	82	D	30–15 ka	W	S	2	Carver and Brook (1989)	Markewich et al. (2015); Conroy et al. (2019)
11	39.5	82	LP	Peoria Loess (30–18 cal ka BP)	W		2	Rutledge et al. (1975)	Muhs and Bettis (2000); Conroy et al. (2019)
12	39	83	LP	Peoria Loess (30–18 cal ka BP)	W		2	Rutledge et al. (1975)	Muhs and Bettis (2000); Conroy et al. (2019)
13	44.5	83.5	D	16.4 to 12.8 ka	W	N	1	Arbogast et al. (2017)	Schaetzl et al. (2018)
14	31.5	84	D	30–15 ka	W		2	Ivester et al. (2001); Ivester and Leigh (2003)	Markewich et al. (2015); Conroy et al. (2019)
15	39.5	84	LP	Peoria Loess (30–18 cal ka BP)	W		2	Rutledge et al. (1975)	Muhs and Bettis (2000); Conroy et al. (2019)
16	41.5	84	D	13.3–8.2 ka	W		1	Campbell et al. (2011)	Schaetzl et al. (2018)
17	45.5	84.5	S	13.3–11.5 ka	E	S	1	Krist and Schaetzl (2001); Shaetzl et al. (2016); Vader et al. (2012)	Schaetzl et al. (2018)
18	44	85	D	13.0–10.1 ka	W	N	1	Arbogast et al. (2015)	Schaetzl et al. (2018)
19	43	86	D	13.3–11.6 ka	W	N	1	Colgan et al. (2017)	Schaetzl et al. (2018)
20	41	86.5	D	15.0–13.0 ka	E	N	1	Kilibarda and Blockland (2011)	Schaetzl et al. (2018)

(*Continued*)

https://doi.org/10.1017/qua.2024.62 Published online by Cambridge University Press

Table 1. (*Continued.*)

	Latitude °N	Longitude °W	Archive Type	Age	Zonal Wind Direction (E or W)	Meridional Wind Direction (N or S)	Confidence Level	Primary Reference(s)	Secondary References
21	41	86.5	D	12.5–11.5 ka	W		1	Kilibarda and Blockland (2011)	Schaetzl et al. (2018)
22	45.5	87	S	13.3–11.5 ka	E	N	1	Shaetzl et al. (2016)	Schaetzl et al. (2018)
23	38	88	LT/LP	Peoria Loess (30–18 ka)	W	N	2	Fehrenbacher et al. (1965); Frazee et al. (1970)	Muhs and Bettis (2000); Conroy et al. (2019)
24	45	88	LT	14–13 ka	E	N	2	Shaetzl et al. (2014)	Schaetzl et al. (2018)
25	45.5	89	LT	14–13 ka	W	N	2	Shaetzl et al. (2014)	Schaetzl et al. (2018)
26	36.5	89.5	LT	Peoria Loess (29–18 ka)	W		2	Rodbell et al. (1997)	Muhs and Bettis (2000); Conroy et al. (2019)
27	38.5	89.5	LT/LP	Peoria Loess (27–15 ka)	W	N	2	Smith (1942); Frazee et al. (1970)	Muhs and Bettis (2000); Conroy et al. (2019)
28	39.5	89.5	LT/LP	Peoria Loess (27–15 ka)	W	N	2	Smith (1942); Frazee et al. (1970)	Muhs and Bettis (2000); Conroy et al. (2019)
29	35.5	90	LT	Peoria Loess (29–18 ka)	W		2	Rodbell et al. (1997)	Muhs and Bettis (2000); Conroy et al. (2019)
30	41.5	90	D	18–15 ka	W	N	1	Miao et al. (2010)	
31	44	90	D	14–10 ka	W	N	1	Rawling et al. (2008)	Schaetzl et al. (2018)
32	32.5	91	LP	Peoria Loess (29–18 ka)	W	N	1	Matalucci et al. (1969); Snowden and Priddy (1968)	Matalucci et al. (1969); Snowden and Priddy (1968)
33	42.5	91	LT/LP	Peoria Loess (27–15 ka)	W		2	Leigh and Knox (1994)	Muhs and Bettis (2000); Conroy et al. (2019)
34	45	91	LT/LC/LP	26–19 ka	W	N	2	Stanley and Schaetzl (2011)	Schaetzl et al. (2018)
35	43.5	91.5	LP	Peoria Loess (27–15 ka)	W	N	1	Mason et al. (1994)	Muhs and Bettis (2000); Conroy et al. (2019)
36	42	92	Dr	Peoria Loess (28–16 cal ka BP)	W	N	1	Hallberg (1979)	Muhs and Bettis (2000); Conroy et al. (2019)
37	44	92	D	12.3–10.3 ka	W	N	2	Hanson et al. (2015)	Schaetzl et al. (2018)
38	45	92	SaSt	11.3–8.9 ka	W	N	1	Shandonay et al. (2022)	
39	39	92.5	LT/LC	Peoria Loess (28–16 cal ka BP)	W		2	Ebens and Connor (1980)	Muhs and Bettis (2000); Conroy et al. (2019)
40	45	93	SaSt	25.3–20.1 ka	W	N	1	Shandonay et al. (2022)	
41	39.5	94	LT/LC	Peoria Loess (28–16 cal ka BP)	W		2	Ebens and Connor (1980)	Muhs and Bettis (2000); Conroy et al. (2019)
42	40.5	95.5	LT/LC	Peoria Loess (28–16 cal ka BP)	W		2	Ebens and Connor (1980)	Muhs and Bettis (2000); Conroy et al. (2019)

(*Continued*)

https://doi.org/10.1017/qua.2024.62 Published online by Cambridge University Press

Table 1. (*Continued.*)

	Latitude °N	Longitude °W	Archive Type	Age	Zonal Wind Direction (E or W)	Meridional Wind Direction (N or S)	Confidence Level	Primary Reference(s)	Secondary References
43	42	95.5	Dr	Peoria Loess (28–16 cal ka BP)	W	N	1	Hallberg (1979)	Muhs and Bettis (2000); Conroy et al. (2019)
44	41	96	LT/LP	Peoria Loess (28–16 cal ka BP)	W		2	Ruhe (1954)	Muhs and Bettis (2000); Conroy et al. (2019)
45	41.5	96	LP/LC	Peoria Loess (28–16 cal ka BP)	W		2	Muhs and Bettis (2000)	Conroy et al. (2019)
46	41	98	LT/LC	Peoria Loess (24–14 cal ka BP)	W	N	2	Mason (2001); Aleinikoff et al. (2008); Mason et al. (2008)	Conroy et al. (2019)
47	42	99	D	15.4–14.9 ka	W	N	1	Mason et al. (2011)	
48	42	99.5	D	14.1 ka	W	N	1	Miao et al. (2007); Mason et al. (2011)	
49	41	100.5	D	24.4–15.5 ka	W	N	1	Mason et al. (2008, 2011)	
50	41.5	100.5	D	18.5–15.6 ka	W	N	1	Mason et al. (2011)	
51	42	100.5	D	17.3 ka	W	N	1	Mason et al. (2011)	
52	40	101	LP	Peoria Loess (24–14 cal ka BP)	W	N	2	Swineford and Frye (1951)	Muhs and Bettis (2000); Conroy et al. (2019)
53	40.5	101	D	13.7–10.7 ka	W	N	1	Mason et al. (2011)	
54	41	101	D	17–14.7 ka	W	N	1	Mason et al. (2011)	
55	42	101	D	16.8–13.5 ka	W	N	1	Miao et al. (2007); Mason et al. (2011)	
56	43	101	D	13.1 ka	W	N	1	Goble et al. (2004)	
57	40.5	101.5	D	14.7 ka	W	N	1	Mason et al. (2011)	
58	41.5	101.5	D	12.9 ka	W	N	1	Mason et al. (2011)	
59	43.5	102.5	D	16.2–12.0 ka	W	N	1	Baldauf et al. (2019)	
60	40	104	LP/LC	Peoria Loess (20–14 ka)	W	N	2	Aleinikoff et al. (1998); Muhs et al. (1999)	Muhs and Bettis (2000); Conroy et al. (2019)
61	42	109.5	D	15.7–14.0 ka	W	S	1	Mayer and Mahan (2004)	
62	55	112	D	12.6 ka	E	S	1	Wolfe et al. (2004)	
63	54	113	D	12.5–11.7 ka	W	N	1	Wolfe et al. (2004)	
64	52.5	113.5	D	12.8–11.3 ka	W	N	1	Wolfe et al. (2004)	
65	53.5	113.5	D	13.4 ka	W	N	1	Wolfe et al. (2004)	
66	55	114	D	15.3–14.2 ka	W	N	1	Wolfe et al. (2004)	
67	54.5	114.5	D	14.5 ka	W	N	1	Wolfe et al. (2004)	
68	60.5	114.5	D	10.5 ka	E	S	1	Wolfe et al. (2004)	
69	52.5	115	D	12.4 ka	W	N	1	Wolfe et al. (2004)	
70	53	115	D	14.1 ka	W	N	1	Wolfe et al. (2004)	
71	54.5	115	D	14.9 ka	W	N	1	Wolfe et al. (2004)	
72	54	116	D	15.7 ka	W	N	1	Wolfe et al. (2004)	

(*Continued*)

https://doi.org/10.1017/qua.2024.62 Published online by Cambridge University Press

Table 1. (*Continued.*)

	Latitude °N	Longitude °W	Archive Type	Age	Zonal Wind Direction (E or W)	Meridional Wind Direction (N or S)	Confidence Level	Primary Reference(s)	Secondary References
73	53.5	116.5	D	14.0 ka	W	N	1	Wolfe et al. (2004)	
74	58.5	116.5	D	13.4–11.7 ka	E	S	1	Wolfe et al. (2007)	
75	58	117	D	11.0–10.3 ka	E	S	1	Wolfe et al. (2007)	
76	55.5	117.5	D	12.9 ka	W		1	Wolfe et al. (2004)	
77	46	118	LT	35–15 ka	W	S	2	Sweeney et al. (2004)	
78	55	118	D	11.8 ka	W		1	Wolfe et al. (2004)	
79	55	118.5	D	14.9 ka	W		1	Wolfe et al. (2004)	
80	55	119	D	13.7–13.5 ka	W		1	Wolfe et al. (2004)	
81	58	121	D	13.9–11.7 ka	W	N	1	Wolfe et al. (2007)	

patterns have long been cited as wind-direction indicators, with thinning and decreasing grain size occurring as one moves away from a source region. The issue at hand is the precision of such interpreted wind direction, because decreasing thickness and grain size downwind typically will parallel the sediment source region as long as wind is blowing from source to area of deposition (Swineford and Frye, 1951; Mason 2001). Additionally, some references note evidence of more variability in inferred wind direction (e.g., the presence of 'secondary' winds from other directions; Fehrenbacher et al., 1965; Thorson and Schile, 1995). Ultimately, loess thickness differences on the western versus eastern margins of river valleys still support interpretations of predominantly eastward transport by westerly winds. However, to accommodate this uncertainty, Table 1 provides two confidence levels that are incorporated into the qualitative agreement metric exercise with the model wind output. Level 1 indicates more robust evidence of past wind direction, such as supplied by dune and spit orientation, and other aeolian features, such as sand stringers. Level 2 indicates more uncertainty in the overall wind direction, with these records mainly coming from loess deposits.

Temporally, we limited our dataset to records that span the LGM (27–19 ka) and the deglaciation (20–11 ka). Similar to the greater uncertainty in loess-inferred wind direction, there is also additional age uncertainty in loess records relative to the more precisely dated dune records. Although many loess sections are well dated using radiocarbon, thermoluminescence, and optically stimulated luminescence methods, some sections of Peoria Loess (Silt) remain only regionally correlated. We thus assigned generalized age ranges to undated Peoria Loess sections from more recent, regional chronology studies (Mason et al., 2008; Muhs et al., 2013; Pigati et al., 2013; Grimley et al., 2024). However, the youngest ages reported may still overestimate the cessation of loess deposition, given they are often below the top of the loess section (Pigati et al., 2013).

For comparison of proxy and model wind direction, we assessed the climatological mean wind directions in 1-ka time slices that match the proxy age. In many cases, the best age estimate or age uncertainty of the archive (deposit or landform) spans a range greater than 1 ka. For archives with age ranges greater than 1 ka, we compared the proxy wind direction versus the model wind direction for all 1-ka time slices that fell within the age window of deposition.

For both zonal and meridional wind direction in the proxy data and mean seasonal model winds at 992.6 hPa (again, the lowest atmospheric level in iTRACE), we calculated a qualitative comparison metric, Gwet's AC1 (Gwet, 2002, 2008). Gwet's AC1 is a type of categorical agreement metric that are increasingly being used in paleoclimate proxy data–model comparisons when the paleoclimate proxy data are qualitative in nature (e.g., DiNezio and Tierney, 2013; Oster et al., 2015, 2023; Conroy et al., 2019). In this work, we assessed the categorical agreement of zonal and meridional wind directions in the proxies and model simulations, which is advantageous as there is often uncertainty in the precise wind direction (i.e., in degrees) in geologic records, but general agreement in the predominant zonal and meridional wind directions (i.e., easterly versus westerly, northerly versus southerly). Gwet's AC1 values range from −1, indicating complete inverse agreement, to 1, indicating complete agreement, with zero indicating no agreement (Tables S1 and S2).We use Gwet's AC1 to assess the strength of proxy data–model agreement in each 1-ka time slice of the deglacial simulation. These values indicate the extent to which the main zonal and meridional wind directions (i.e., westerly versus easterly and northerly versus southerly) in the proxy data and model simulation agree. This particular metric is useful because it also accounts for the probability of chance agreement in a set of proxy data–model comparison points (Gwet, 2002). All proxy data in Table 1 contain a qualitative indication of zonal wind direction (e.g., 'W'), but not all have a meridional component (e.g., 'N'). Thus, we calculated Gwet's AC1 for the meridional direction only for those data points that had an inferred meridional direction. In each 1-ka time slice, Gwet's AC1 agreement metrics were calculated for each season, given the seasonality of aeolian wind-direction proxies is uncertain. This does not assume that we considered all seasons as likely times of proxy formation, which is further assessed in the discussion.

Results

The majority of the proxy wind-direction data compiled here indicate westerly and northwesterly winds during the LGM and through the deglaciation (Table 1 and Fig. 1). Fewer records indicate a southerly or easterly component. Of all 81 records spanning some portion of the LGM and deglaciation, 71 (88%) are westerly and 10 (12%) are easterly. These inferred easterly winds are mainly interpreted from the orientation of lacustrine spits in the Upper Midwest and New England (synthesized in Schaetzl et al., 2018) and the orientation of dunes in Alberta and Saskatchewan (Wolfe et al., 2004, 2007) after 15 ka.

In the iTRACE simulation, the climate of the deglaciation is defined by the loss of ice sheets in the Northern Hemisphere,

https://doi.org/10.1017/qua.2024.62 Published online by Cambridge University Press

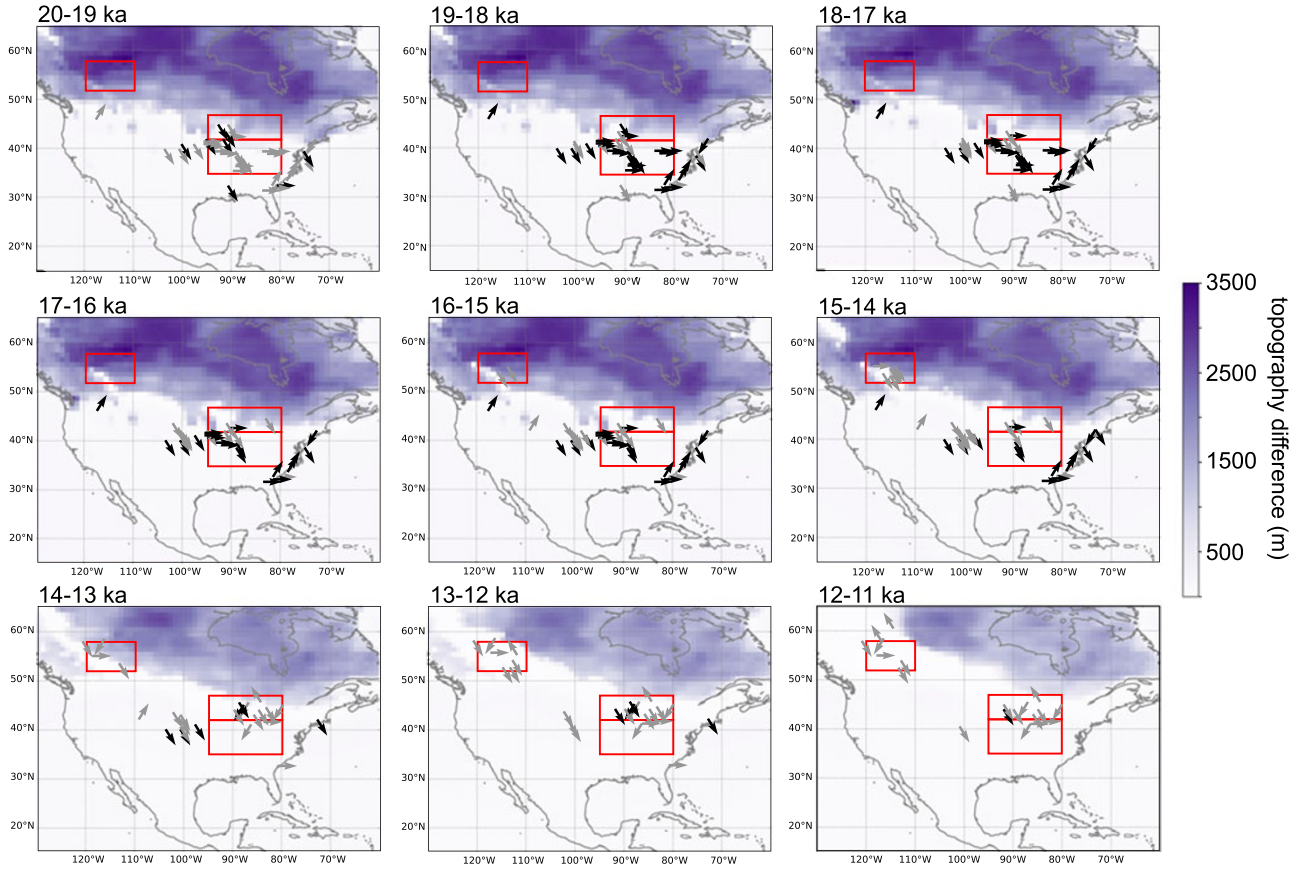

Figure 1. One-thousand-year time interval maps spanning the last deglaciation from 20 ka to 12 ka showing the ICE_6G_C Laurentide and Cordilleran ice sheets, expressed as topographic difference in meters relative to modern (Peltier et al., 2015). Vectors (not to scale) summarize the near-surface zonal and meridional wind directions from proxy records in Table 1 with ages spanning the 1000-year time intervals. Gray color vectors indicate greater confidence in direction, as explained in the methods section. Red boxes (Western Canada, Upper Midwest, Lower Midwest) indicate averaged regions plotted as time series (Figures 6b–d).

leading to higher surface temperatures over the formerly ice-covered regions due to the change in land surface properties. Regional cooling occurs during millennia with substantial meltwater forcing (Figs. 1 and S1). The Laurentide High, a stationary area of high SLP over the ice sheet that reflects near-surface circulation and thus sets wind directions (red-hued contours in Figs. 2–4, and S2), also decreases in magnitude and spatial extent as the ice retreats. Simulated winds at 992.6 hPa (henceforth 'near-surface winds') reveal substantial spatial and seasonal variations in wind strength and direction across North America. There is strong northerly flow near the ice sheet margin in winter, spring, and fall, which can be easterly or westerly depending on longitude and season (Fig. 2). South of the ice margin, winds are weaker, and again vary in direction depending on season and location. By the end of the deglaciation (12–11 ka), when the ice sheet is restricted to areas closer to Hudson Bay, near-surface winds are weaker over previously glaciated areas. The zonal component of the winds is more westerly in winter and easterly in summer over central North America (Fig. 4). Strong northeasterly winds are located along the retreating ice sheet margin (Figs. 1 and 4).

Gwet's AC1 values across 1-ka intervals of the last deglaciation allowed us to assess more directly how well proxy and model wind directions agree in different seasons in both the zonal and meridional directions (Fig. 5). At 20 ka, representing the closest approximation to the LGM boundary conditions, Gwet's AC1 values are quite high for zonal winds in winter and spring (Fig. 5a). Zonal proxy data–model wind direction agreement is weaker in summer and fall, with more easterly model winds at 20 ka. Between 16 ka and 12 ka, zonal proxy data–model wind-direction agreement decreases in winter and spring, but increases in fall, with summer agreement remaining negative or near zero. There are fewer points of comparison for meridional winds, but agreement is very high in winter, spring, and fall from 20–15 ka. Agreement weakens from 15–12 ka in winter, spring, and fall, but increases for summer. These general patterns of agreement through time are similar when assessing all the proxy data in Table 1, as well as only those data with more robust wind direction and chronology information (thick versus thin lines in Fig. 5).

To further assess temporal variability in regional wind speed and direction in iTRACE, we evaluated the variability in decadal (10-year) annual average near-surface zonal and meridional winds from 20–11 ka for the regions of the Lower Midwest, Upper Midwest, and Western Canada (red boxes in Figs. 1 and 6). These are regions that contain many of the proxy wind-direction records. In the Lower Midwest (35–42°N, 80–95°W), a region with abundant loess thickness and particle size records supporting westerly to northwesterly winds during the LGM, simulated zonal winds remain westerly throughout the last deglaciation, but westerly wind speeds abruptly weaken at points during the end of HS1 and in the Bølling–Allerød (Fig. 6b). Westerly winds become consistently weaker after 13 ka. Simulated meridional winds

https://doi.org/10.1017/qua.2024.62 Published online by Cambridge University Press

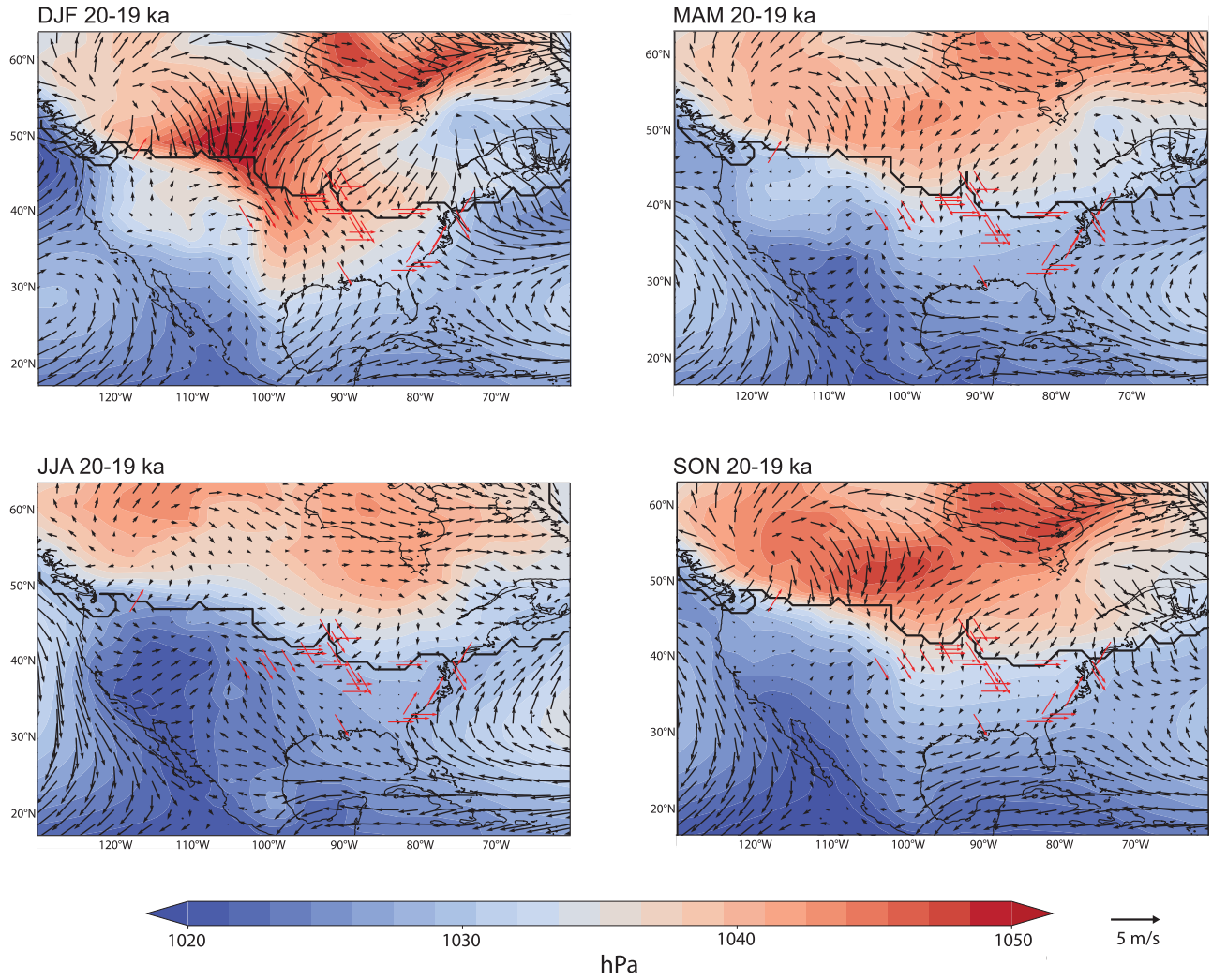

Figure 2. iTRACE maps of seasonal average sea level pressure (SLP) and near-surface winds (black vectors) over North America at 20 ka. Red vectors are proxy vectors from Figure 1 with chronologies overlapping 20 ka. Thick solid line indicates ice sheet limit, expressed as ice fraction >100%. DJF = December, January, February; MAM = March, April, May; JJA = June, July, August; SON = September, October, November.

are consistently northerly but weaken steadily throughout the deglaciation (Fig. 6b).

In the Upper Midwest (42–47°N, 80–95°W), where lacustrine spits support easterly winds near the ice margin during the last deglaciation, we observed simulated northeasterly winds from 20–11 ka in iTRACE. However, there are also aeolian archives that point to westerly to northwesterly prevailing winds within the Upper Midwest during this time. Authors have interpreted these regional data to collectively indicate some katabatic easterly flow off the adjacent ice margin, which diminished over a short distance from the ice margin (~150 km) where the winds became consistently westerly (Arbogast et al., 2015; Schaetzl et al., 2018). In iTRACE, the northeasterly winds over this region through the deglaciation are perhaps too strong and spatially pervasive, although they do steadily weaken from 20–11 ka (Fig. 5). Thus, for the Lower and Upper Midwest there is some proxy data–model agreement regarding wind direction, but the latitude of surface wind-direction transition from easterly to westerly seems to be farther south (i.e., the boundary between the 'Upper Midwest' and 'Lower Midwest' boxes) in the model relative to the proxy archives.

In western Canada (52–58°N, 110–120°W), dune orientation shows evidence for both westerly and easterly wind directions with local retreat of the ice sheet. From 16 ka to 13 ka, inferred surface winds from dunes were dominantly westerly to northwesterly, with some indication of more easterly and southeasterly winds from 13–9 ka (Wolfe et al., 2004, 2007). These easterly to southeasterly winds are again attributed to anticyclonic flow associated with the Laurentide High, as well as katabatic winds off the ice sheet positioned to the northeast of the dune sites (Wolfe et al., 2004). Across this region, annual average simulated zonal wind direction was westerly until 16 ka. Zonal wind speed weakened from 18–16 ka, when it became easterly. Prevailing easterly winds then weakened between 14 ka and 12 ka. Meridional winds were consistently northerly in this region until 14 ka, after which they abruptly became southerly. Thus, this model supports transitions from dominantly northwesterly to southeasterly winds in this region, although the timing of this shift to easterly winds is earlier in the model than in the dunes.

Near-surface wind anomalies, calculated as the difference between the simulations with and without meltwater forcing, also reveal the effect of high latitude meltwater forcing on near-surface

https://doi.org/10.1017/qua.2024.62 Published online by Cambridge University Press

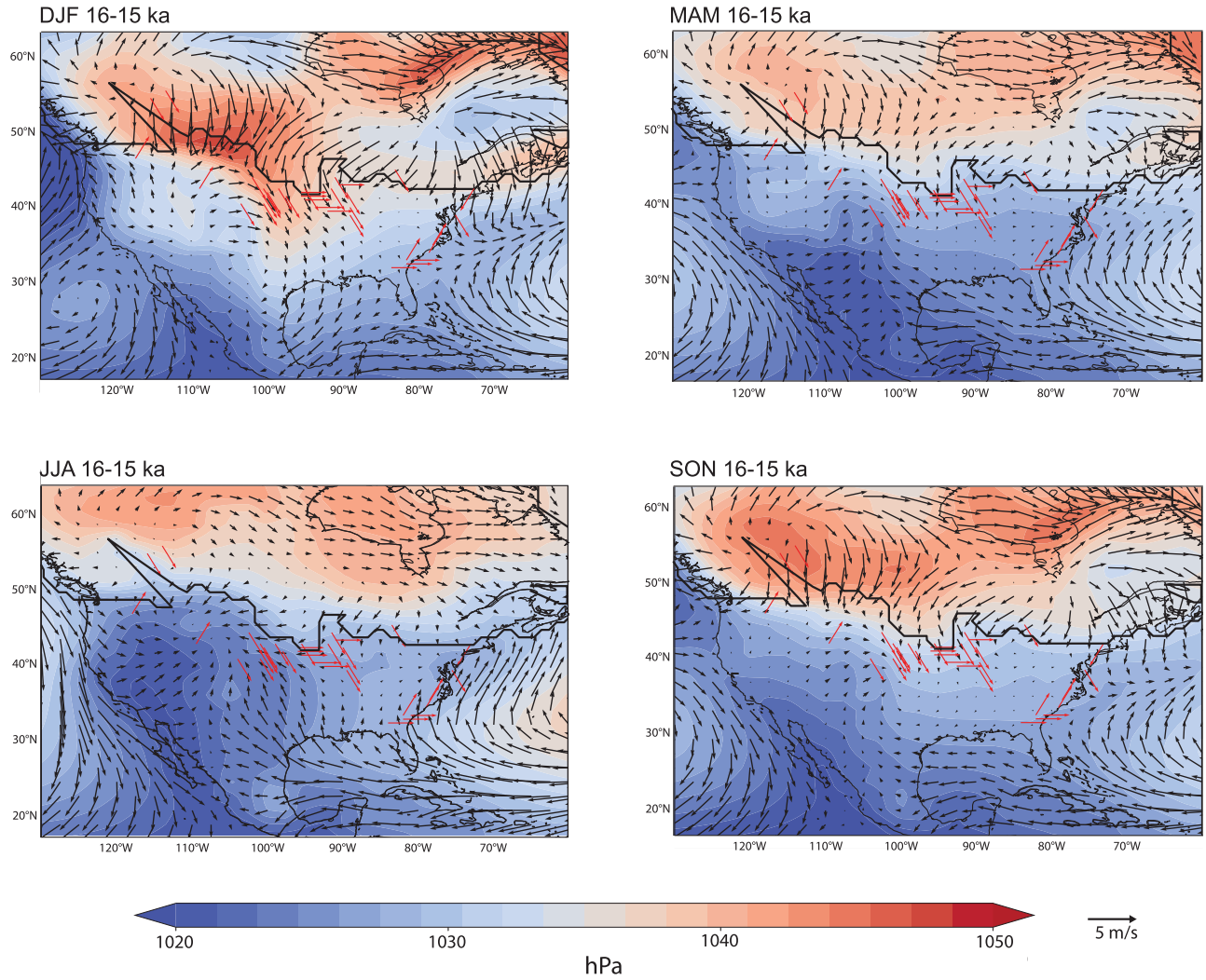

Figure 3. iTRACE maps of seasonal average sea level pressure (SLP) and near-surface winds (black vectors) over North America as in Figure 2, but at 16 ka. Red vectors are proxy vectors from Figure 1 with chronologies overlapping 16 ka. Thick solid line indicates ice sheet limit, expressed as ice fraction >100%. DJF = December, January, February; MAM = March, April, May; JJA = June, July, August; SON = September, October, November.

winds toward the latter part of the last deglaciation. We observed the largest differences in near-surface winds over the oceans with the addition of meltwater forcing, especially in the North Atlantic in association with changes in ocean temperature and land–ocean sea level pressure gradients (Figs. 7, S3, and S4). At 16 ka, this results in anomalous easterly onshore flow into eastern North America (Fig. 7).

Discussion

Ice sheet influence on near-surface winds through the deglaciation

The presence of continental ice sheets is well established as a key control on both large-scale glacial atmospheric circulation (Löfverström et al., 2014; Ullman et al., 2014; Izumi et al., 2023) and regional glacial climates (Griggs et al., 2022, Thomas et al., 2023). Thus, it is not surprising that many observed deglacial trends in climate over northern North America in the iTRACE simulation are associated with ice sheet retreat, although near-surface wind-direction changes with ice sheet retreat have not been investigated as commonly with transient climate model simulations. As SLP decreases over the Laurentide Ice Sheet (Fig. 6a), associated near-surface anticyclonic flow moves northeastward, tracking the retreating ice (Figs. 2–4). This manifests as weakening northeasterly winds over the upper Midwestern United States (Fig. 6c). Furthermore, an abrupt transition from northwesterly to southeasterly winds in western Canada at 14 ka also coincides with the North American 'Saddle Collapse,' or the separation of the Laurentide and Cordilleran ice sheets, which affected the large-scale zonal circulation from the northeastern Pacific to the North Atlantic (Löfverström and Lora, 2017; Lora et al., 2017). However, abrupt shifts in SLP every 1 ka are due to the implementation of different ice sheets every 1 ka, and thus the timing and abruptness of SLP and associated wind shifts (Fig. 6) should not be interpreted precisely as abrupt climate events in the simulation. Regardless, they do demonstrate that retreat of the Laurentide Ice Sheet appears to be a strong influence on near-surface winds in regions with proxy wind-direction records, such as in the Upper Midwest and western Canada (Fig. 6).

https://doi.org/10.1017/qua.2024.62 Published online by Cambridge University Press

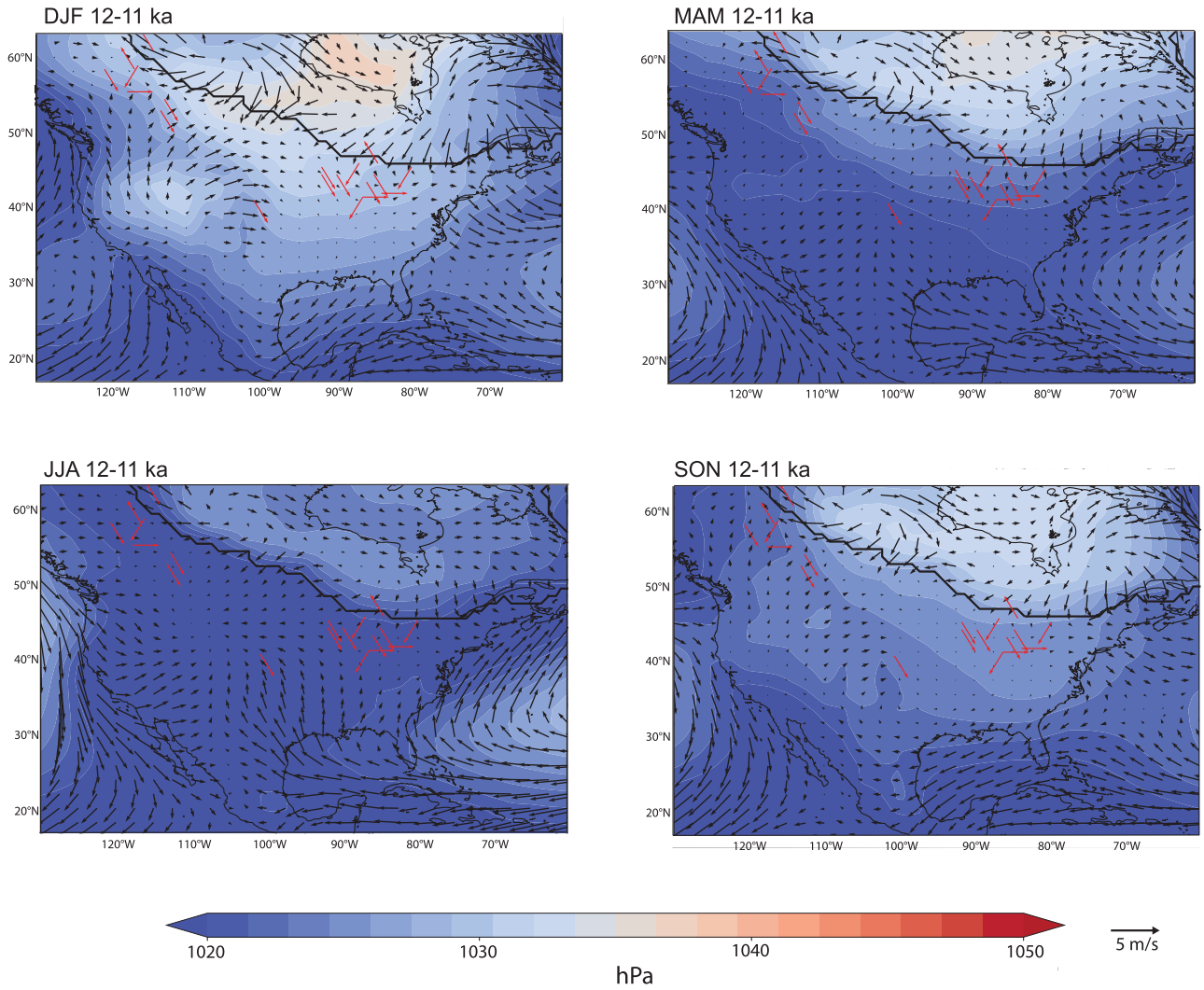

Figure 4. iTRACE maps of seasonal average sea level pressure (SLP) and near-surface winds (black vectors) over North America as in Figures 2 and 3, but at 12 ka. Red vectors are proxy vectors from Figure 1 with chronologies overlapping 12 ka. Thick solid line indicates ice sheet limit, expressed as ice fraction >100%. DJF = December, January, February; MAM = March, April, May; JJA = June, July, August; SON = September, October, November.

The cause of these changes in near-surface winds with ice sheet retreat may be due to related changes in the footprint of the Laurentide High and related anticyclonic circulation. Past LGM simulations have shown that near-surface anticyclonic circulation of the Laurentide High leads to northeasterly winds near the glacial ice margin in North America (Kutzbach and Guetter, 1986; COHMAP Members, 1988; Bromwich et al., 2004). More recent LGM simulations show a range of Laurentide High 'footprints' that vary across different models, which influences the location and strength of northeasterly flow near the ice margin (Conroy et al., 2019). However, changes in the size and extent of the ice sheet itself may also influence near-surface winds if they are katabatic in nature.

The northeasterly winds in iTRACE also do not always align with areas of high SLP, and instead seem to coincide with the ice margin and with anticyclonic flow around the areas of highest ice elevation (rather than highest SLP). Recent work comparing winds over the Fennoscandian Ice Sheet in CCSM3 versus CESM1 has shown that higher resolution models have ice sheets that are able to "create their own wind-regimes," including katabatic winds (Schenk and Vineusa, 2019). Similarly, an older simulation of LGM winter using a higher resolution regional Polar MM5 model also captured katabatic flow off the Laurentide Ice Sheet margin (Bromwich et al., 2004). In iTRACE, above 912 hPa, winds in midcontinental North America are largely westerly (Fig. 8). This further supports the hypothesis that the near-surface northeasterly winds in iTRACE are katabatic in nature, given that high-density katabatic winds would likely be found nearer to the surface.

The relationship between the upper-level westerly winds and near-surface winds across North America

Inquiries into the nature and drivers of glacial and deglacial atmospheric circulation anomalies over North America focus heavily on the location and strength of the mid-latitude jet stream (e.g., Oster et al., 2015, Lora et al., 2017). The location of the jet stream is frequently implicated in driving hydroclimatic anomalies, although

https://doi.org/10.1017/qua.2024.62 Published online by Cambridge University Press

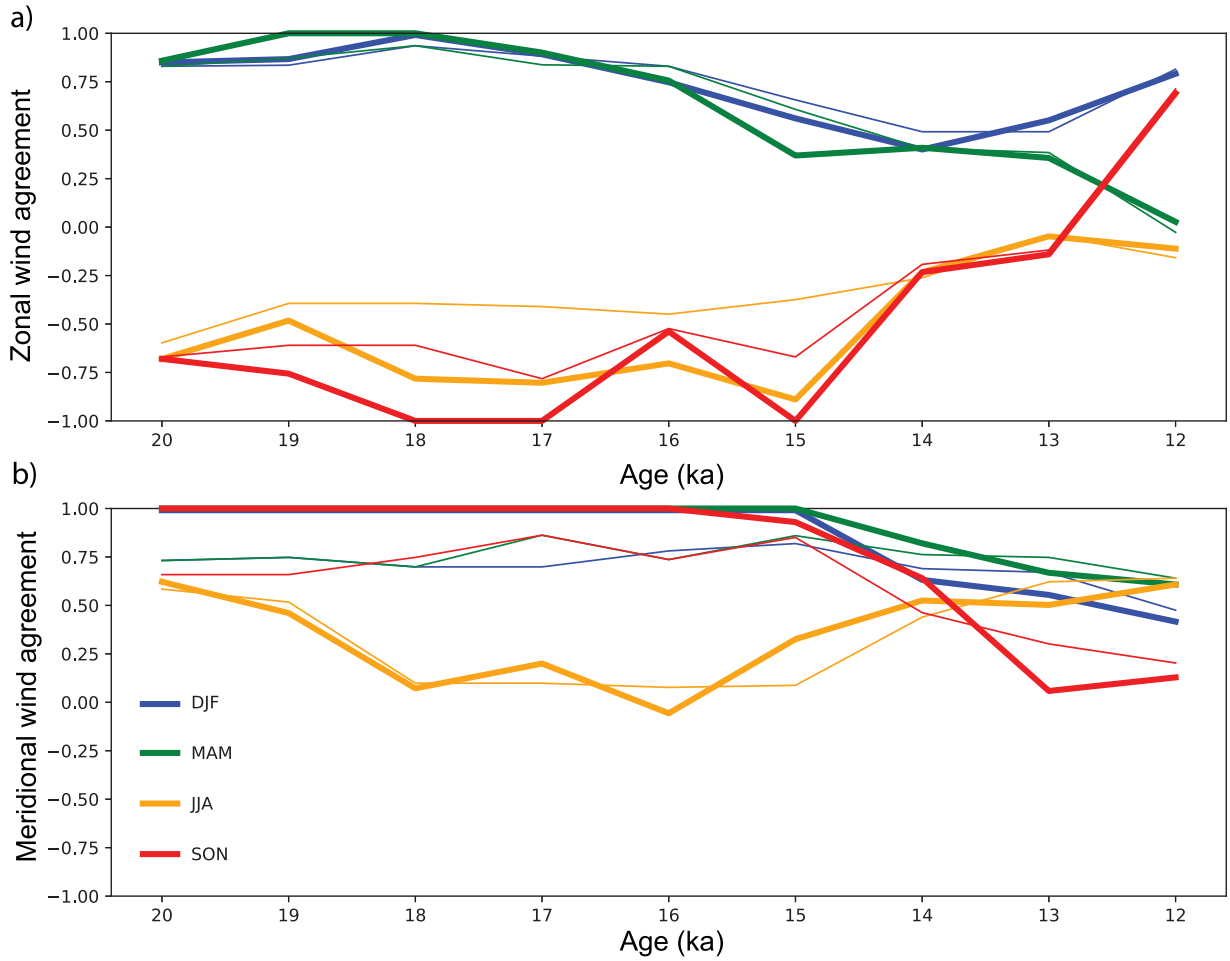

Figure 5. Gwet's AC1 agreement values for proxy and seasonal model (a) zonal and (b) meridional wind directions in each 1-ka interval from 20 ka to 12 ka. Colors indicate agreement in different model seasons of boreal winter (DJF), spring (MAM), summer (JJA), and fall (SON), as indicated in the legend. Thinner lines are agreement values for all proxy data with chronologies that fall within a given 1-ka time period, thicker lines are agreement values for the more robust records of paleowind direction only (confidence level of 1 in Table 1).

the intensity of moisture transport may also be an important consideration (Lora et al., 2017). Considering surface wind-direction proxy records, a more southward jet stream has also been hypothesized to contribute to the archived westerly wind directions in midcontinental loess deposits. A southward-displaced jet stream may have steered storms with a strong, westerly wind component over the region. Strong winds associated with these infrequent storms may have entrained silt and led to its downwind deposition in loess deposits (Muhs and Bettis, 2000). In this case, the westerly wind direction preserved in loess deposits would then be biased toward high frequency, storm-associated, wind directions (Muhs and Bettis, 2000). We cannot examine this hypothesis at the required temporal resolution with the monthly resolved iTRACE simulation, but we can assess the relationship between monthly averaged and climatological near-surface winds and the upper-level westerly winds through the troposphere during the deglaciation, which can help us assess the strength of the relationship between the upper-level westerlies and near-surface winds.

As previously discussed, the near-surface easterly winds over parts of North America, such as along the ice margin, are not persistent at higher levels in the troposphere (Fig. 8). Put another way, seasonally, the strong westerly winds aloft that correspond to the jet stream do not always extend to the surface. This is also observed by the weak, and even negative, correlation coefficients between near-surface zonal winds (at 992.6 hPa) and upper-level winds (at 197.9 hPa, near the peak westerly wind speeds of the jet stream) across much of midcontinental North America (Fig. S5). Thus, it is challenging to consistently link the observed changes in near-surface wind directions in our areas of focus to the jet stream using the monthly iTRACE output. However, the faster upper-level westerlies do appear to expand at 90°W to cover a greater latitudinal extent as deglaciation proceeds, which may have climatic implications that warrant further investigation in future studies (Fig. 8).

Meltwater pulses and near-surface wind anomalies

In the Lower Midwest region (Fig. 6b), zonal, near-surface wind variability shows a temporal pattern that appears to be independent of the weakening trend in the Laurentide High as deglaciation proceeds. Here, westerly winds strengthen and weaken in spurts during HS1, the Bølling–Allerød, and the Younger Dryas. Examining the iTRACE simulations without meltwater forcing suggests that meltwater forcing may be the cause of this variability. When assessing the difference in winds and SLP in 1-ka simulations with and without meltwater forcing, we found strong anomalies in SLP over

https://doi.org/10.1017/qua.2024.62 Published online by Cambridge University Press

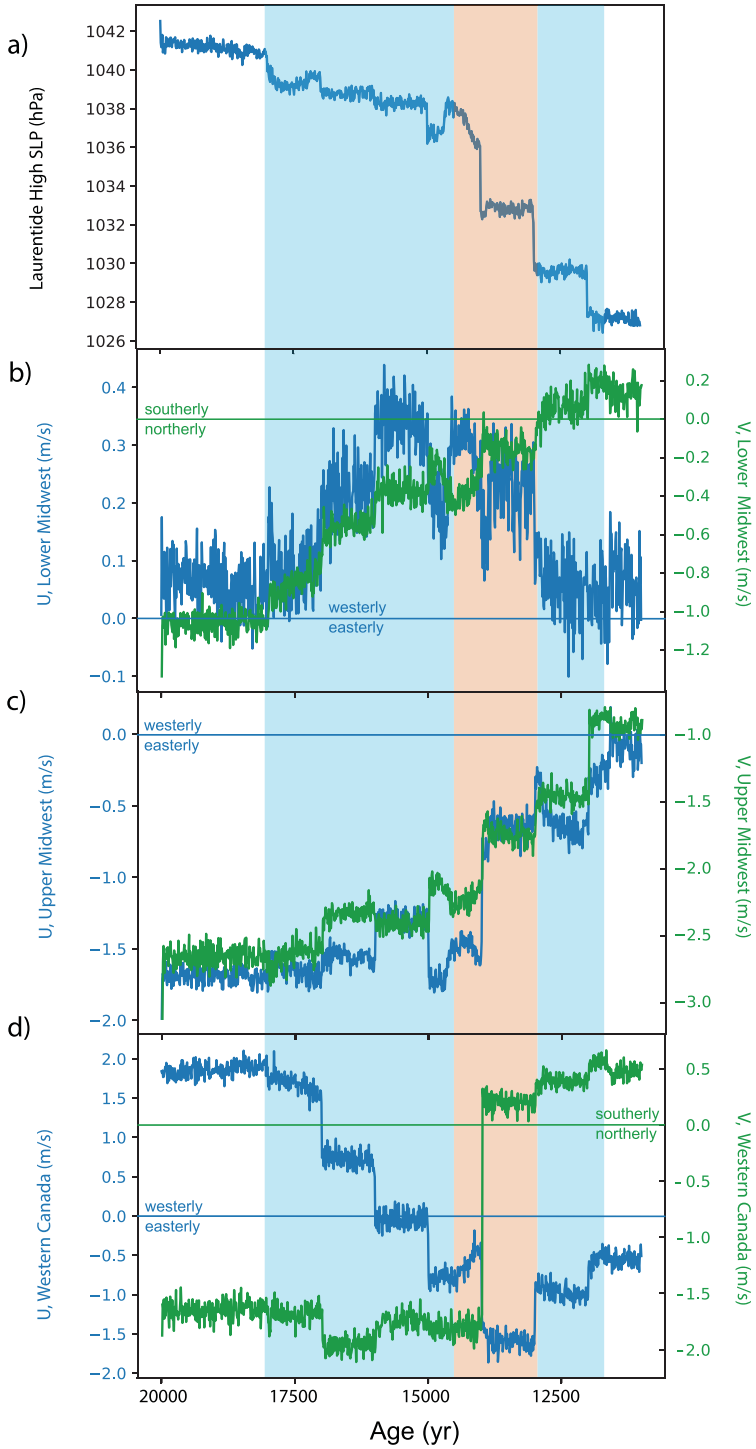

Figure 6. (a) Time series of 10-year average annual sea level pressure (SLP) within the Laurentide High area (45–55°N, 110–80°W), (b) 10-year average annual near-surface zonal ('U,' blue) and meridional ('V,' green) wind speed between 35–42°N, 80–95°W ('Lower Midwest'), (c) 10-year average annual near-surface zonal (blue) and meridional (green) wind speed between 42–47°N, 80–95°W ('Upper Midwest'), (d) 10-year average annual near-surface zonal (blue) and meridional (green) wind speed between 52–58°N, 110–120°W ('Western Canada'). Blue shaded intervals represent Heinrich event 1 (18–14.5 ka) and the Younger Dryas (12.9–11.7 ka). Orange shading represents the Bølling–Allerød (14.5–12.9 ka).

North America and the North Atlantic connected closely to near-surface wind anomalies. Using the 16-ka period as an example, when Northern Hemisphere meltwater forcing was strongest, we observed weak, low SLP anomalies over North America, with adjacent strong, high SLP anomalies over the North Atlantic (Fig. 7). These high SLP anomalies over the North Atlantic are due to colder waters associated with the meltwater fluxes into the ocean that weakened Atlantic Meridional Overturning Circulation. The resulting pressure gradient leads to anomalous near-surface easterly to northeasterly flow from the Atlantic onto the eastern North American continent, especially in winter. A similar pattern is seen in the 13-ka period (Fig. S3). We also observed strong southwesterly wind anomalies along the west coast of North America at 16 ka due to this meltwater forcing, similar to the findings of Oster et al. (2023). Within the three wind-direction proxy 'study areas', the strongest meltwater influence was seen in the Lower Midwest

https://doi.org/10.1017/qua.2024.62 Published online by Cambridge University Press

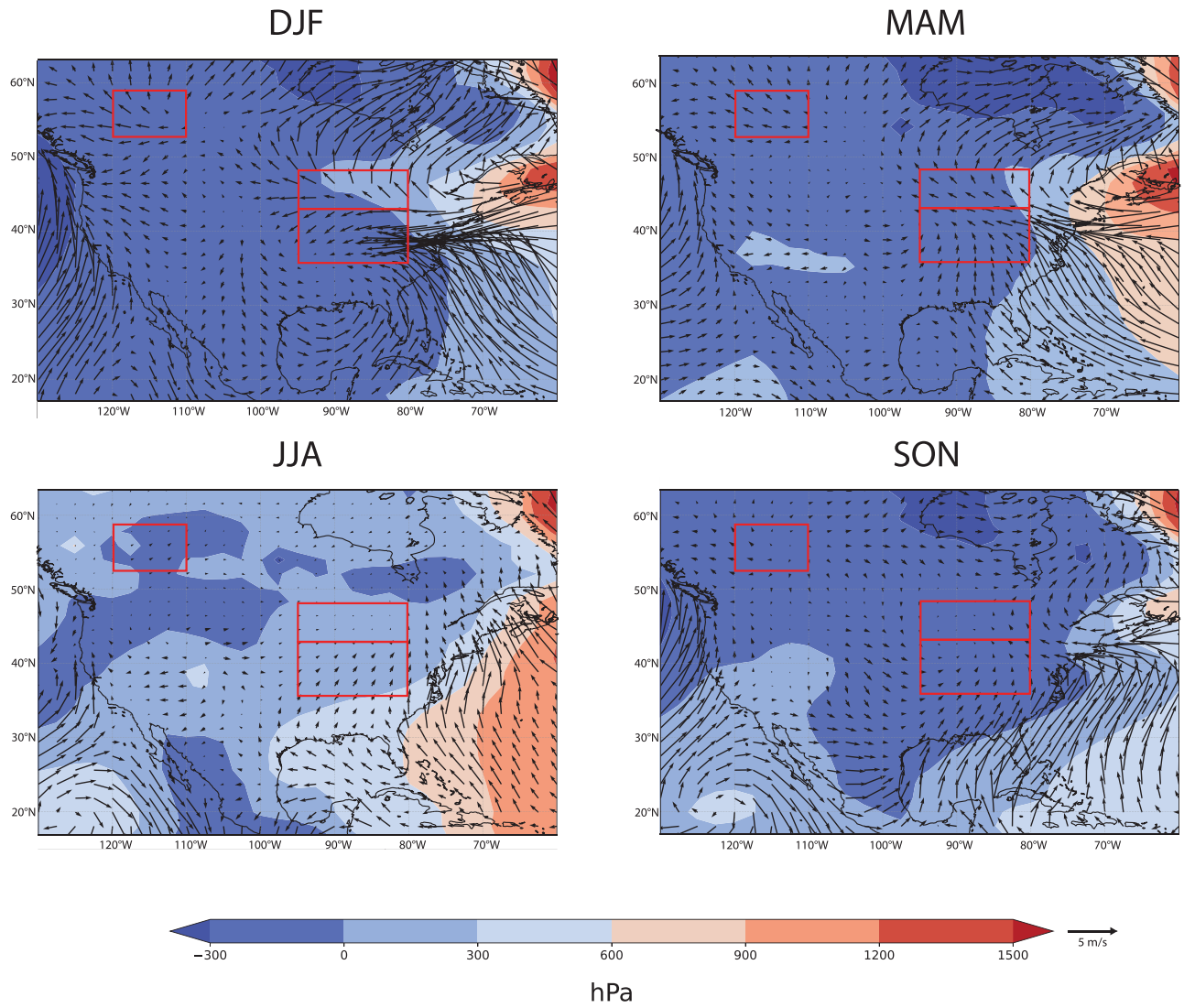

Figure 7. Meltwater forcing (ICE+ORB+GHG+MW – ICE+ORB+GHG) seasonal anomaly (difference) maps of low-level winds and SLP at 16 ka. Red boxes (Western Canada, Upper Midwest, Lower Midwest) indicate averaged regions plotted as time series (Figure 6b–d and S4b–d). ICE = ICE-6G-C dataset; ORB = orbital forcing of radiation; GHG = atmospheric greenhouse gas (CO_2, CH_4, N_2O) concentrations; MW = meltwater fluxes.

in winter, with large easterly wind anomalies, indicating that periods of abrupt westerly wind weakening observed in iTRACE in the Lower Midwest region are likely related to meltwater forcing (Figs. 7 and S4). Thus, while simulated easterly to northeasterly winds near the southeastern Laurentide ice margin seem to be a result of anticyclonic flow and/or katabatic flow off the ice sheet, these individual forcing experiments also reveal a role for meltwater forcing in producing near-surface changes in winds during deglaciation. However, in this case, excluding meltwater forcing does not substantially change our AC1 proxy–data model agreement values, because meltwater forcing influences wind speed more so than direction.

Proxy–model agreement in near-surface wind direction, and implications for proxy wind interpretations

Gwet's AC1 results, summarized above, show strong agreement in many 1 ka periods between model and proxy-inferred wind directions (Fig. 5). This is encouraging and supports previous conclusions regarding the extent of westerly winds during the LGM and the deglaciation, but also the existence of some easterly winds close to the ice margin (Schaetzl et al., 2018), which can also be seen in Figures 2–4. Only using the more robust proxy wind-direction interpretations in the calculation of the agreement metrics does not substantially alter our conclusions (Fig. 5). This indicates that qualitative, categorical zonal and meridional wind-direction interpretations from features such as loess thickness patterns are sound, even if they lack the precision of dune-inferred wind directions.

The seasonality of aeolian wind-direction proxies, or the season in which they were deposited, is uncertain, so our comparison of the 'season-independent' proxy wind directions with seasonal model wind directions is a useful exercise to help identify this seasonality in the proxy data. The higher seasonal agreement metrics in winter, spring, and fall suggest these may be the primary seasons of wind-driven aeolian deposition, perhaps due to factors such as faster winds and wind gusts in these seasons (Conroy et al., 2019). Spring and fall in particular may have been a likely time of high aeolian activity when cyclogenesis and cold fronts may have aligned to produce favorable wind conditions for sand and

https://doi.org/10.1017/qua.2024.62 Published online by Cambridge University Press

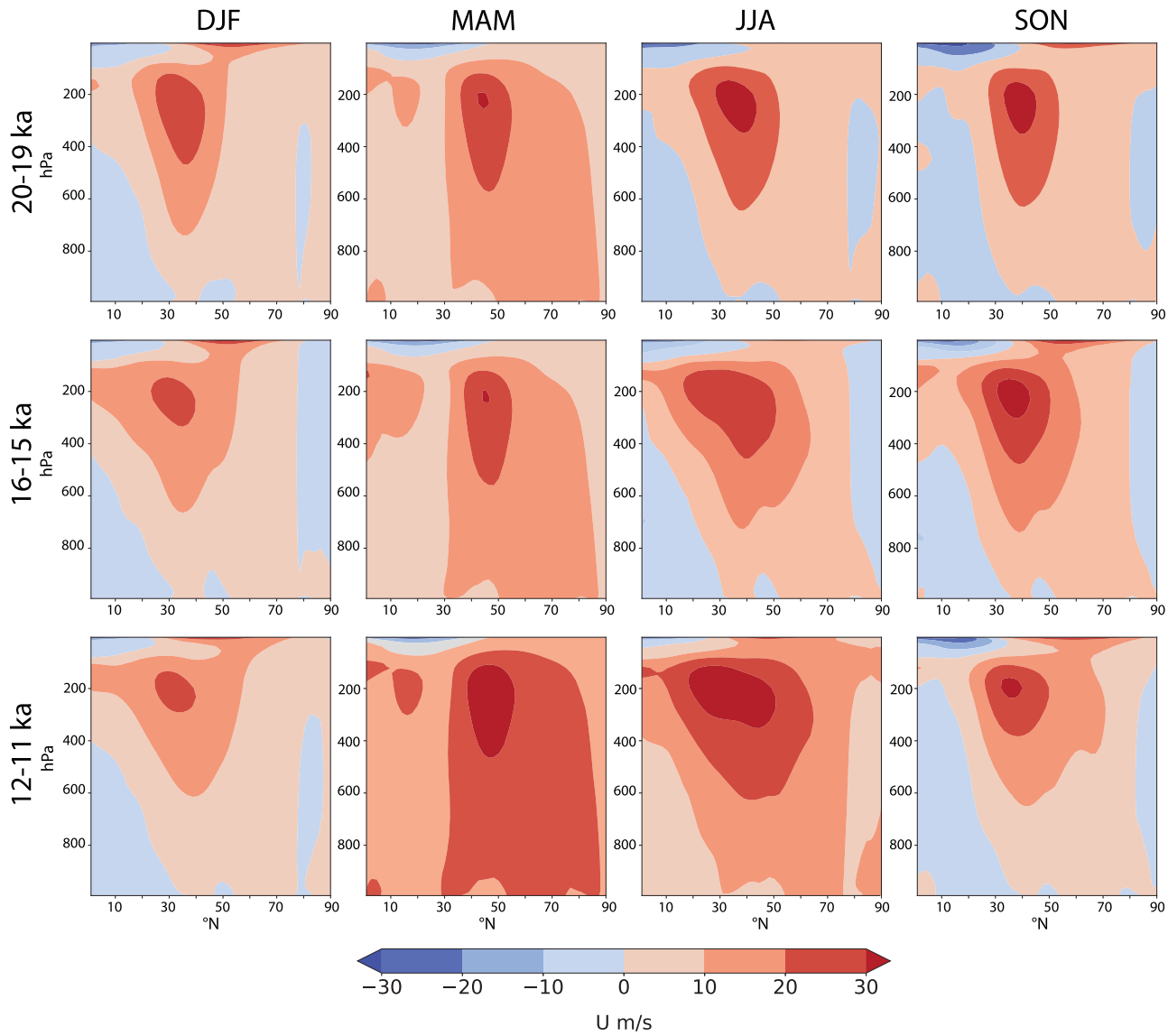

Figure 8. Seasonal average zonal wind speed through the atmosphere (in hPa) at 90°W (close to Mississippi River Valley at 30–45°N) from 0–90°N at 20–19 ka, 16–15 ka, and 12–11 ka. Red shading indicates westerly winds, blue shading indicates easterly winds.

silt transport (Roe, 2009; Bullard and Mockford, 2018). However, many other factors (in addition to wind and wind gust velocity), such as soil moisture, snow cover, frozen ground, river flooding extent, and stabilizing vegetation can also influence the ability of sediment to be deflated or mobilized by wind (Orgill and Sehmel, 1976; Crusius et al., 2011; Bullard, 2013; Bullard et al., 2016; Bullard and Mockford, 2018).

Zonal wind agreement metrics decrease in winter and spring and increase in fall as deglaciation proceeds (Fig. 5). Meridional wind agreement also shows deglacial trends, with summer agreement decreasing then increasing, and fall, winter, and spring agreement decreasing after 15 ka. These shifts could suggest a change in the predominant seasons of aeolian activity in the latter part of the deglaciation. One overarching reason for such a change in the season of aeolian activity in the study region may be the waning influence of the Laurentide High. With the diminishing footprint of anticyclonic circulation, and katabatic winds, especially in winter and spring later in the deglaciation, other climate factors may have become more important in leading to the conditions for aeolian activity. Wind speeds also decrease in central North America in winter, spring, and fall at 12 ka relative to 20 ka and 16 ka (Figs. 2–4). However, the change in the main season of strong proxy–model agreement could also simply indicate a change in the representation of locations and types of wind-direction proxy in the dataset. For example, Upper Midwestern lacustrine spit data, which date to the latter part of the deglaciation, appear to be warm season-biased, because they require wind-driven currents to form, and hence, unfrozen lake surfaces. Notably, after 15 ka when these records begin, there is an increase in summer and fall agreement metrics for zonal wind directions (Fig. 5), perhaps pointing to this warm season bias in the dataset.

The proxy–model comparison presented here is a means of ground-truthing wind direction in paleoclimate simulations, but the iTRACE simulations can also provide insight into causes of the timing and cessation of aeolian activity, as observed from the geologic record, throughout the deglaciation. For example, from

https://doi.org/10.1017/qua.2024.62 Published online by Cambridge University Press

16 ka to 12 ka wind speeds decrease across midcontinental North America, in winter, spring, and fall (Figs. 3 and 4). During this time interval, Great Plains aeolian systems stabilized (Mason et al., 2008). Although this stabilization is hypothesized to be a result of increasing moisture availability and warmer temperatures, near-surface wind data from iTRACE suggests lower wind speeds also may have been a factor. In contrast, in the Upper Midwest, winds remain stronger later in the deglacial period, and there is also geologic evidence for later aeolian activity, around the Younger Dryas (e.g., Campbell et al., 2011; Schaetzl et al., 2018).

Conclusions

Deglacial near-surface winds in the iTRACE simulations agree with the geologic evidence of northeasterly to easterly winds near the retreating southern margin of the Laurentide Ice Sheet during the last deglaciation. These near-surface winds were likely a result of both katabatic flow off the ice sheet and anticyclonic flow associated with the Laurentide High. However, model wind direction is predominantly westerly at higher elevations in the atmosphere and south of the ice margin. Thus, modeled and paleodata-based wind-direction inferences still support westerly to northwesterly winds across much of the North American midcontinent. The latitude of transition from easterly to westerly near-surface winds does seem to extend farther south of the transition near the ice margin in iTRACE than indicated by various paleowind-direction records. Future high spatial resolution transient deglacial experiments, for example, with a regional model, may be necessary to address this limitation.

There are also sizable differences in zonal and meridional wind speeds through the deglaciation in the iTRACE simulation with the addition of meltwater pulses incorporated into the model forcing. In particular, along the eastern seaboard, easterly wind anomalies are associated with meltwater forcing in the North Atlantic at 16 ka and 13 ka and their influence on temperature and pressure gradients in the region. Thus, this might be a promising area to investigate meltwater-driven terrestrial climate anomalies in future studies.

The promising agreement between many proxy-inferred wind-direction records and near-surface model wind directions, especially in winter and spring, is encouraging and suggests the prescribed forcing factors in iTRACE are robust. However, the footprint and strength of the Laurentide High and near-surface wind direction depend on modeled ice sheet topography, which varies substantially in different ice sheet model generations (Peltier et al., 2015; Conroy et al., 2019). Additionally, because meltwater fluxes appear to meaningfully influence near-surface winds in certain areas, conclusions regarding meltwater forcing depend on complete knowledge of the timing, magnitude, and location of these fluxes. Overall, this proxy data–model comparison of wind direction through the deglaciation supports the complexity of proxy-inferred wind-direction changes and offers additional insight into the drivers and seasonality of past changes in near-surface wind direction in North America.

Supplementary material. The supplementary material for this article can be found at https://doi.org/10.1017/qua.2024.62.

Acknowledgments. We are grateful to Chengfei He and colleagues for the production and public dissemination of the iTRACE simulation data, as well as to Joe Mason, Tom Lowell, and an anonymous reviewer for their helpful comments that improved this paper. JLC and CK acknowledge funding for this work from NSF-AGS-2202919 and NSF-AGS-2202920. The authors declare no competing interests. Data analysis was done with NCAR's Computational and Information Systems Laboratory.

References

Aleinikoff, J.N., Muhs, D.R., Fanning, C.M., 1998. Isotopic evidence for the sources of late Wisconsin (Peoria) loess, Colorado and Nebraska: implications for paleoclimate. In: Busacca, A.J. (Ed.), *Dust Aerosols, Loess Soils and Global Change*. Washington State Univ. College of Agriculture and Home Economics, Pullman, WA, pp. 124–127.

Aleinikoff, J.N., Muhs, D.R., Bettis, E.A., Johnson, W.C., Fanning, C.M., Benton, R., 2008. Isotopic evidence for the diversity of late Quaternary loess in Nebraska: glaciogenic and nonglaciogenic sources. *Geological Society of America Bulletin* **120**, 1362–1377.

Arbogast, A.F., Luehmann, M.D., Miller, B.A., Wernette, P.A., Adams, K.M., Waha, J.D., O'Neil, G.A., *et al.*, 2015. Late-Pleistocene paleowinds and aeolian sand mobilization in north-central Lower Michigan. *Aeolian Research* **16**, 109–116.

Arbogast, A.F., Luehmann, M.D., Monaghan, G.W., Lovis, W.A., Wang, H., 2017. Paleoenvironmental and geomorphic significance of bluff-top dunes along the Au Sable River in northeastern Lower Michigan, USA. *Geomorphology* **297**, 112–121.

Baldauf, P.E., Burkhart, P.A., Hanson, P.R., Miles, M., Larsen, A., 2019. Chronology of dune development in the White River Badlands, northern Great Plains, USA. *Aeolian Research* **37**, 14–24.

Brady, E., Stevenson, S., Bailey, D., Liu, Z., Noone, D., Nusbaumer, J., Otto-Bliesner, B.L., *et al.*, 2019. The connected isotopic water cycle in the Community Earth System Model Version 1. *Journal of Advances in Modeling Earth Systems* **11**, 2547–2566.

Bromwich, D.H., Toracinta, E.R., Wei, H., Oglesby, R.J., Fastook, J.L., Hughes, T., 2004. Polar MM5 simulations of the winter climate of the Laurentide Ice Sheet at the LGM. *Journal of Climate* **17**, 3415–3433.

Bullard, J.E., 2013. Contemporary glacigenic inputs to the dust cycle. Earth Surface Processes and Landforms **38**, 71–89.

Bullard, J.E., Mockford, T., 2018. Seasonal and decadal variability of dust observations in the Kangerlussuaq area, west Greenland. *Arctic, Antarctic, and Alpine Research* **50**, S100011. https://doi.org/10.1080/15230430.2017.1415854

Bullard, J.E., Baddock, M., Bradwell, T., Crusius, J., Darlington, E., Gaiero, D., Gasso, S., *et al.*, 2016. High-latitude dust in the Earth system. *Reviews of Geophysics* **54**, 447–485.

Campbell, M.C., Fisher, T.G., Goble, R.J., 2011. Terrestrial sensitivity to abrupt cooling recorded by aeolian activity in northwest Ohio, USA. *Quaternary Research* **75**, 411–416.

Carver, R.E., Brook, G.A., 1989. Late Pleistocene paleowind directions, Atlantic Coastal Plain, U.S.A. *Palaeogeography, Palaeoclimatology, Palaeoecology* **74**, 205–216.

Clark, P.U., Dyke, A.S., Shakun, J.D., Carlson, A.E., Clark, J., Wohlfarth, B., Mitrovica, J.X., Hostetler, S.W., McCabe, A.M., 2009. The last glacial maximum. *Science* **325**, 710–714.

COHMAP Members, 1988. Climatic changes of the last 18,000 years: observations and model simulations. *Science* **241**, 1043–1052.

Colgan, P.M., Amidon, W.H., Thurkettle, S.A., 2017. Inland dunes on the abandoned bed of Glacial Lake Chicago indicate eolian activity during the Pleistocene–Holocene transition, southwestern Michigan, USA. *Quaternary Research* **87**, 66–81.

Conroy, J.L., Karamperidou, C., Grimley, D.A., Guenthner, W.R., 2019. Surface winds across eastern and midcontinental North America during the last glacial maximum: a new data-model assessment. *Quaternary Science Reviews* **220**, 14–29.

Crusius, J., Schroth, A.W., Gasso, S., Moy, C.M., Levy, R.C., Gatica, M., 2011. Glacial flour dust storms in the Gulf of Alaska: hydrologic and meteorological controls and their importance as a source of bioavailable iron. *Geophysical Research Letters* **38**, L06602, https://doi.org/10.1029/2010GL046573

DiNezio, P.N., Tierney, J.E., 2013. The effect of sea level on glacial Indo-Pacific climate. *Nature Geoscience* **6**, 485–491.

Ebens, R.J., Connor, J.J., 1980. Geochemistry of loess and carbonate residuum: geochemical survey of Missouri. *U.S. Geological Survey Professional Paper* **954-G**, 31 p.

Fehrenbacher, J.B., White, J.L., Ulrich, H.P., Odell, R.T., 1965. Loess distribution in southeastern Illinois and southwestern Indiana. *Soil Science Society of America Proceedings* **29**, 566–572.

Frazee, C.J., Fehrenbacher, J.B., Krumbein, W.C., 1970. Loess distribution from a source. *Soil Science Society of America Proceedings* **34**, 296–301.

Goble, R.J., Mason, J.A., Loope, D.B., Swinehart, J.B., 2004. Optical and radiocarbon ages of stacked paleosols and dune sands in the Nebraska Sand Hills, USA. *Quaternary Science Reviews* **23**, 1173–1182.

Griggs, C.B., Lewis, C.M., Kristovich, D.A., 2022. A late-glacial lake-effect climate regime and abundant tamarack in the Great Lakes Region, North America. *Quaternary Research* **109**, 83–101.

Grimley, D.A., Loope, H.M., Jacobs, P.M., Nash, T.A., Dendy, S.N., Conroy, J.L., Curry, B.B., 2024. Updated chronology for Peoria Silt (loess) accumulation in Illinois and western Indiana from radiocarbon dating of terrestrial gastropod shells. *Quaternary Research* **121**, 40–58.

Gwet, K., 2002. Kappa statistic is not satisfactory for assessing the extent of agreement between raters. *Statistical Methods For Inter-Rater Reliability Assessment* **1**, 1-5.

Gwet, K.L., 2008. Computing inter-rater reliability and its variance in the presence of high agreement. *British Journal of Mathematical and Statistical Psychology* **61**, 29–48.

Hallberg, G.R., 1979. Wind-aligned drainage in loess in Iowa. *Proceedings of the Iowa Academy of Science* **86**, 4–9.

Hanson, P., Mason, J., Jacobs, P., Young, A., 2015. Evidence for bioturbation of luminescence signals in eolian sand on upland ridgetops, southeastern Minnesota, USA. *Quaternary International* **362**, 108–115.

He, C., Liu, Z., Otto-Bliesner, B.L., Brady, E.C., Zhu, C., Tomas, R., Clark, P.U., *et al.*, 2021. Hydroclimate footprint of pan-Asian monsoon water isotope during the last deglaciation. *Science Advances* **7**, eabe2611. https://doi.org/10.1126/sciadv.abe2611

Hurrell, J.W., Holland, M.M., Gent, P.R., Ghan, S., Kay, J.E., Kushner, P.J., Lamarque, J.-F., *et al.*, 2013. The Community Earth System Model: a framework for collaborative research. *Bulletin of the American Meteorological Society* **94**, 1339–1360.

Ivester, A.H., Leigh, D.S., 2003. Riverine dunes on the Coastal Plain of Georgia, USA. *Geomorphology* **51**, 289–311.

Ivester, A.H., Leigh, D.S., Godfrey-Smith, D.I., 2001. Chronology of inland eolian dunes on the Coastal Plain of Georgia, USA. *Quaternary Research* **55**, 293–302.

Izumi, K., Valdes, P., Ivanovic, R., Gregoire, L., 2023. Impacts of the PMIP4 ice sheets on Northern Hemisphere climate during the last glacial period. *Climate Dynamics* **60**, 2481–2499.

Karnauskas, K.B., Lundquist, J.K., Zhang, L., 2018. Southward shift of the global wind energy resource under high carbon dioxide emissions. *Nature Geoscience* **11**, 38–43.

Kilibarda, Z., Blockland, J., 2011. Morphology and origin of the Fair Oaks Dunes in NW Indiana, USA. *Geomorphology* **125**, 305–318.

Krist, F., Schaetzl, R.J., 2001. Paleowind (11,000 BP) directions derived from lake spits in northern Michigan. *Geomorphology* **38**, 1–18.

Kutzbach, J.E., Guetter, P.J., 1986. The influence of changing orbital parameters and surface boundary conditions on climate simulations for the past 18 000 years. *Journal of the Atmospheric Sciences* **43**, 1726–1759.

Leigh, D.S., Knox, J.C., 1994. Loess of the Upper Mississippi Valley driftless area. *Quaternary Research* **42**, 30–40.

Liu, Z., Otto-Bliesner, B.L., He, F., Brady, E.C., Tomas, R., Clark, P.U., Carlson, A.E., *et al.*, 2009. Transient simulation of last deglaciation with a new mechanism for Bølling–Allerød warming. *Science* **325**, 310–314.

Löfverström, M., Lora, J.M., 2017. Abrupt regime shifts in the North Atlantic atmospheric circulation over the last deglaciation. *Geophysical Research Letters* **44**, 8047–8055.

Löfverström, M., Caballero, R., Nilsson, J., Kleman, J., 2014. Evolution of the large-scale atmospheric circulation in response to changing ice sheets over the last glacial cycle. *Climate of the Past* **10**, 1453–1471.

Lora, J.M., Mitchell, J.L., Tripati, A.E., 2017. Abrupt reorganization of North Pacific and western North American climate during the last deglaciation. *Geophysical Research Letters* **43**, 11,796–11,804.

Markewich, H.W., Litwin, R.J., Wysocki, D.A., Pavich, M.J., 2015. Synthesis on Quaternary aeolian research in the unglaciated eastern United States. *Aeolian Research* **17**, 139–191.

Martinez, A., Iglesias, G., 2022. Climate change impacts on wind energy resources in North America based on the CMIP6 projections. *Science of the Total Environment* **806**, 150580. https://doi.org/10.1016/j.scitotenv.2021.150580

Mason, J.A., 2001. Transport direction of Peoria Loess in Nebraska and implications for loess sources on the central Great Plains. *Quaternary Research* **56**, 79–86.

Mason, J.A., Nater, E.A., Hobbs, H.C., 1994. Transport direction of Wisconsinan loess in southeastern Minnesota. *Quaternary Research* **41**, 44–51.

Mason, J.A., Miao, X., Hanson, P.R., Johnson, W.C., Jacobs, P.M., Goble, R.J., 2008. Loess record of the Pleistocene–Holocene transition on the northern and central Great Plains, USA. *Quaternary Science Reviews* **27**, 1772–1783.

Mason, J.A., Swinehart, J.B., Hanson, P.R., Loope, D.B., Goble, R.J., Miao, X., Schmeisser, R.L., 2011. Late Pleistocene dune activity in the central Great Plains, USA. *Quaternary Science Reviews* **30**, 3858–3870.

Matalucci, R.V., Shelton, J.W., Abdelhad, M., 1969. Grain orientation in Vicksburg Loess. *Journal of Sedimentary Petrology* **39**, 969–979.

Mayer, J.H., Mahan, S.A., 2004. Late Quaternary stratigraphy and geochronology of the western Killpecker Dunes, Wyoming, USA. *Quaternary Research* **61**, 72–84.

McVicar, T.R., Roderick, M.L., Donohue, R.J., Li, L.T., Van Niel, T.G., Thomas, A., Grieser, J., *et al.*, 2012. Global review and synthesis of trends in observed terrestrial near-surface wind speeds: implications for evaporation. *Journal of Hydrology* **416–417**, 182–205.

Miao, X., Mason, J.A., Johnson, W.C., Wang, H., 2007. High-resolution proxy record of Holocene climate from a loess section in southwestern Nebraska, USA. *Palaeogeography, Palaeoclimatology, Palaeoecology* **245**, 368–381.

Miao, X., Hanson, P.R., Wang, H., Young, A.R., 2010. Timing and origin for sand dunes in the Green River Lowland of Illinois, upper Mississippi River Valley, USA. *Quaternary Science Reviews* **29**, 763–773.

Muhs, D.R., Bettis, E.A., 2000. Geochemical variations in Peoria Loess of western Iowa indicate paleowinds of midcontinental North America during last glaciation. *Quaternary Research* **53**, 49–61.

Muhs, D.R., Aleinikoff, J.N., Stafford, T.W., Kihl, R., Been, J., Mahan, S.A., Cowherd, S.D., 1999. Late Quaternary loess in northeastern Colorado, I: age and paleoclimatic significance. *Geological Society of America Bulletin* **111**, 1861–1875.

Muhs, D.R., Bettis, E.A., Roberts, H.M., Harlan, S.S., Paces, J.B., Reynolds, R.L., 2013. Chronology and provenance of last-glacial (Peoria) loess in western Iowa and paleoclimatic implications. *Quaternary Research* **80**, 468–481.

Orgill, M.M., Sehmel, G.A., 1976. Frequency and diurnal variation of dust storms in the contiguous USA. *Atmospheric Environment (1967)* **10**, 813–825.

Oster, J.L., Ibarra, D.E., Winnick, M.J., Maher, K., 2015. Steering of westerly storms over western North America at the last glacial maximum. *Nature Geoscience* **8**, 201–205. https://doi.org/10.1038/ngeo2365

Oster, J.L., Macarewich, S., Lofverstrom, M., de Wet, C., Montañez, I., Lora, J.M., Skinner, C., Tabor, C., 2023. North Atlantic meltwater during Heinrich Stadial 1 drives wetter climate with more atmospheric rivers in western North America. *Science Advances* **9**, eadj2225. https://doi.org/10.1126/sciadv.adj2225

Peltier, W.R., Argus, D.F., Drummond, R., 2015. Space geodesy constrains ice age terminal deglaciation: the global ICE-6G_C (VM5a) model. *Journal of Geophysical Research: Solid Earth* **120**, 450–487.

Pigati, J.S., McGeehin, J.P., Muhs, D.R., Bettis, E.A, 2013. Radiocarbon dating Late Quaternary loess deposits using small terrestrial gastropod shells. *Quaternary Science Reviews* **76**, 114–128.

Rawling, J.E., Hanson, P., Young, A.R., Attig, J.W., 2008. Late Pleistocene dune construction in the central sand plain of Wisconsin, USA. *Geomorphology* **100**, 494–505.

https://doi.org/10.1017/qua.2024.62 Published online by Cambridge University Press

Rodbell, D.T., Forman, S.L., Pierson, J., Lynn, W.C., 1997. Stratigraphy and chronology of Mississippi Valley loess in western Tennessee. *Geological Society of America Bulletin* **109**, 1134–1148.

Roe, G., 2009. On the interpretation of Chinese loess as a paleoclimate indicator. *Quaternary Research* **71**, 150–161.

Ruhe, R.V., 1954. Relations of the properties of Wisconsin loess to topography in western Iowa. *American Journal of Science* **252**, 663–672.

Rutledge, E.M., Holowaychuk, N., Hall, G.F., Wilding, L.P., 1975. Loess in Ohio in relation to several possible source areas: I. physical and chemical properties. *Soil Science Society of America Proceedings* **39**, 1125–1132.

Schaetzl, R.J., Forman, S.L., Attig, J.W., 2014. Optical ages on loess derived from outwash surfaces constrain the advance of the Laurentide Ice Sheet out of the Lake Superior Basin, USA. *Quaternary Research* **81**, 318–329.

Schaetzl, R.J., Krist, F.J., Lewis, C.M., Luehmann, M.D., Michalek, M.J., 2016. Spits formed in Glacial Lake Algonquin indicate strong easterly winds over the Laurentian Great Lakes during Late Pleistocene. *Journal of Paleolimnology* **55**, 49–65.

Schaetzl, R.J., Larson, P.H., Faulkner, D.J., Running, G.L., Jol, H.M., Rittenour, T.M., 2018. Eolian sand and loess deposits indicate west–northwest paleowinds during the Late Pleistocene in western Wisconsin, USA. *Quaternary Research* **89**, 769–785.

Schenk, F., Vinuesa, R., 2019. Enhanced large-scale atmospheric flow interaction with ice sheets at high model resolution. *Results in Engineering* **3**, 100030. https://doi.org/10.1016/j.rineng.2019.100030

Shandonay, K.L., Bowen, M.W., Larson, P.H., Running, G.L., Rittenour, T., Mataitis, R., 2022. Morphology and stratigraphy of aeolian sand stringers in southeast Minnesota and western Wisconsin, USA. *Earth Surface Processes and Landforms* **47**, 2863–2876.

Smith, G.D., 1942. Illinois loess: variations in its properties and distribution, a pedologic interpretation. *University of Illinois Agricultural Experiment Station Bulletin* **490**, 139–184.

Snowden, J.O., Priddy, R.R., 1968. Geology of Mississippi loess. *Mississippi Geological Survey Bulletin* **111**, 13–203.

Stanley, K.E., Schaetzl, R.J., 2011. Characteristics and paleoenvironmental significance of a thin, dual-sourced loess sheet, north-central Wisconsin. *Aeolian Research* **2**, 241–251.

St. George, S., Wolfe, S.A., 2009. El Niño stills winter winds across the southern Canadian Prairies. *Geophysical Research Letters* **36**, L23806. https://doi.org/10.1029/2009GL041282

Sweeney, M.R., Mason, J.A., 2013. Mechanisms of dust emission from Pleistocene loess deposits, Nebraska, USA. *Journal of Geophysical Research-Earth Surface* **118**, 1460–1471.

Sweeney, M.R., Busacca, A.J., Richardson, C.A., Blinnikov, M., McDonald, E.V., 2004. Glacial anticyclone recorded in Palouse loess of northwestern United States. *Geology* **32**, 705–708.

Sweeney, M., Etyemezian, V., Macpherson, T., Nickling, W., Gillies, J., Nikolich, G., McDonald, E., 2008. Comparison of PI-SWERL with dust emission measurements from a straight-line field wind tunnel. *Journal of Geophysical Research: Earth Surface* **113**, F01012. https://doi.org/10.1029/2007JF000830

Swezey, C.S., Schultz, A.P., González, W.A., Bernhardt, C.E., Doar W.R., Garrity, C.P., Mahan, S.A., McGeehin, J.P., 2013. Quaternary eolian dunes in the Savannah River valley, Jasper County, South Carolina, USA. *Quaternary Research* **80**, 250–264.

Swineford, A., Frye, J.C., 1951. Petrography of the Peoria Loess in Kansas. *Journal of Geology* **59**, 306–322.

Thomas, E.K., Cluett, A.A., Erb, M.P., McKay, N.P., Briner, J.P., Castañeda, I.S., Corcoran, M.C., Cowling, O.C., Gorbey, D.B., Lindberg, K.R., 2023. Early Holocene Laurentide Ice Sheet retreat influenced summer atmospheric circulation in Baffin Bay. *Geophysical Research Letters* **50**, e2023GL103428. https://doi.org/10.1029/2023GL103428

Thorson, R.M., Schile, C.A., 1995. Deglacial eolian regimes in New England. *Geological Society of America Bulletin* **107**, 751–761.

Ullman, D.J., LeGrande, A.N., Carlson, A.E., Anslow, F.S., Licciardi, J.M., 2014. Assessing the impact of Laurentide Ice Sheet topography on glacial climate. *Climate of the Past* **10**, 487–507.

Vader, M.J., Zeman, B.K., Schaetzl, R.J., Anderson, K.L., Walquist, R.W., Freiberger, K.M., Emmendorfer, J.A., Wang, H., 2012. Proxy evidence for easterly winds in Glacial Lake Algonquin, from the Black River Delta in northern Lower Michigan. *Physical Geography* **33**, 252–268.

Vimpere, L., 2023. Parabolic dune distribution, morphology and activity during the last 20 000 years: a global overview. *Earth Surface Processes and Landforms* **49**, 117–146. https://doi.org/10.1002/esp.5648

Wolfe, S., Huntley, D., Ollerhead, J., 2004. Relict Late Wisconsinan dune fields of the Northern Great Plains, Canada. *Géographie Physique et Quaternaire* **58**, 323–336.

Wolfe, S.A., Paulen, R.C., Smith, I.R., Lamothe, M., 2007. Age and paleoenvironmental significance of Late Wisconsinan dune fields in the Mount Watt and Fontas River map areas, northern Alberta and British Columbia. *Geological Survey of Canada, Current Research* **2007–B4**, 10. https://doi.org/10.4095/223690

Wolfe, S.A., Demitroff, M., Neudorf, C.M., Woronko, B., Chmielowska-Michalak, D., Lian, O.B., 2023. Late Quaternary eolian dune-field mobilization and stabilization near the Laurentide Ice Sheet limit, New Jersey Pine Barrens, eastern USA. *Aeolian Research* **62**, 100877. https://doi.org/10.1016/j.aeolia.2023.100877

Zeng, Z., Ziegler, A.D., Searchinger, T., Yang, L., Chen, A., Ju, K., Piao, S., *et al.*, 2019. A reversal in global terrestrial stilling and its implications for wind energy production. *Nature Climate Change* **9**, 979–985.

https://doi.org/10.1017/qua.2024.62 Published online by Cambridge University Press